Respiratory Research

RESEARCH

Open Access

Chronic diesel exhaust exposure induced pulmonary vascular remodeling a potential trajectory for traffic related pulmonary hypertension

Chaohui Mu[1†], Qinghai Li[1,2,3†], Yong Niu[4†], Ting Hu[1], Yanting Li[3], Tao Wang[2], Xinjuan Yu[2], Yiqiao Lv[5], Huiling Tang[5], Jing Jiang[6], Haibin Xu[7], Yuxin Zheng[3*] and Wei Han[1,2,3*]

Abstract

Background As one of the most common traffic-related pollutants, diesel exhaust (DE) confers high risk for cardiovascular and respiratory diseases. However, its impact on pulmonary vessels is still unclear.

Methods To explore the effects of DE exposure on pulmonary vascular remodeling, our study analyzed the number and volume of small pulmonary vessels in the diesel engine testers (the DET group) from Luoyang Diesel Engine Factory and the controls (the non-DET group) from the local water company, using spirometry and carbon content in airway macrophage (CCAM) in sputum. And then we constructed a rat model of chronic DE exposure, in which 12 rats were divided into the DE group (6 rats with 16-week DE exposure) and the control group (6 rats with 16-week clean air exposure). During right heart catheterization, right ventricular systolic pressure (RVSP) was assessed by manometry. Macrophage migration inhibitory factor (MIF) in lung tissues and bronchoalveolar lavage fluid (BALF) were measured by qRT-PCR and ELISA, respectively. Histopathological analysis for cardiovascular remodeling was also performed.

Results In DET cohort, the number and volume of small pulmonary vessels in CT were positively correlated with CCAM in sputum ($P<0.05$). Rat model revealed that chronic DE-exposed rats had elevated RVSP, along with increased wall thickness of pulmonary small vessels and right the ventricle. What's more, the MIF levels in BALF and lung tissues were higher in DE-exposed rats than the controls.

Conclusion Apart from airway remodeling, DE also induces pulmonary vascular remodeling, which will lead to cardiopulmonary dysfunction.

†Chaohui Mu, Qinghai Li and Yong Niu contributed equally to this work.

*Correspondence:
Yuxin Zheng
yxzheng@qdu.edu.cn
Wei Han
hanw@qdu.edu.cn

Full list of author information is available at the end of the article

Keywords Diesel exhaust, Pulmonary vascular remodeling, Carbon content in airway macrophage, Wall thickness of small pulmonary vessel, CT

Introduction

Diesel engines are widely used in various sectors such as transportation, mining, and shipping due to their advantages of strong power and cost-effectiveness. However, diesel exhaust (DE) is also considered as a significant contributor to air pollution [1, 2], chronic exposure to DE can bring various diseases, including respiratory, circulatory, neurological, and reproductive disorders, and even increase the risk of malignant tumors [3–6].

Since the respiratory system is the first target of DE exposure, individuals with DE exposure are more susceptible to various chronic airway diseases, such as chronic obstructive pulmonary disease (COPD), asthma, and lung cancer [7, 8].A previous controlled study in humans demonstrated that acute exposure to DE increased the pulmonary vascular resistance in healthy participants [9]. Epidemiological studies had showed that ambient particulate matter exposure is associated with increased right ventricular diastolic pressure and increased right ventricular mass [10, 11]. Diesel exhaust particles are one of the main components of PM2.5 in urban environments [12, 13]. Animal experiments have shown that environmental fine particulate matter can aggravate pulmonary artery vasoconstriction and pulmonary artery wall thickening [14–16], as well as increase pulmonary artery pressure by echocardiography [17], suggesting that environmental particulate matter, mainly diesel exhaust particles, may cause pulmonary hypertension or right heart failure by promoting pulmonary vascular remodeling. However, due to the limitations of related examination technology, we still lack direct evidence of the impact of environmental particulate matter, mainly DE, on human pulmonary vessels.

In recent years, with the recent advances in CT imaging technology, thin-section CT combined with automated image analysis has been used for the quantitative evaluation of airways and pulmonary vessels in chronic airway diseases and a series of artificial intelligence platform have been established [18–21]. Currently, these platforms are primarily applied to the detection of COPD [22–24] and idiopathic pulmonary fibrosis [25]. However, there is still a lack of research on pulmonary vascular structure in the population exposed to DE.

A unique cohort of occupational DE exposure in DETs has been established since 2012 [26] and followed up in 2018, 2023 when a series of respiratory specific examinations, including chest CT and spirometry, were added [27]. In this study, we compared the chest CT scan images and spirometry parameters between DETs and controls in 2018 to explore the pulmonary vascular health consequences of DE exposure. Additionally, we also investigated the characteristics and possible mechanisms of DE exposure-induced pulmonary vascular remodeling in rats to provide a scientific basis for targeted protective measures.

Materials and methods

Study participants

In 2018, our researchers recruited 78 diesel engine testers (the DET group) from Luoyang Diesel Engine Factory and 76 controls (the non-DET group) from the local water company to form a DET cohort. The inclusion and exclusion criteria, as well as the collection of baseline information were described in detail in the previously published articles of our research group [26, 28, 29]. During the data collection process, 10 participants with high image noise in chest CT could not be analyzed ant thus were excluded. Finally, a total of 78 DETs and 66 non-DETs were included in this study.

Written informed consent was obtained from all participants prior to interviews and any procedures. The protocol was approved by the Medical Ethics Review Committee of the Institute for Occupational Health and Poison Control, Chinese Center for Disease Control and Prevention (Protocol No.: NIOHP201604).

Environmental exposure assessments

The levels of fine particulate matter (PM2.5), PM2.5-related elemental carbon (EC), organic carbon (OC), and total carbon (TC) within the DET workshops and local water company were assessed during our 2018 follow-up visit. Detailed methods can be found elsewhere [30]. Our measurements of PM2.5-related EC, OC and TC in the DET group and the control group were presented in a previous study [31].

Carbon content in airway macrophage (CCAM) measurements

CCAM is a biomarker for internal exposure to DE, and we can estimate the DE exposure by quantifying the CCAM. The detailed processes of sputum collection, processing, slide preparation, and quality assessment for both the DET and non-DET groups were described in a previous study [32]. For each subject, 50 macrophages with intact cytoplasm and clear nuclear staining were randomly selected to calculate the proportion of the cytoplasmic area occupied by carbon particles. Before quantifying the carbon particles and cytoplasmic area, we removed the nuclei to account for any potential bias caused by the overlap of macrophages and DEP particles

with nuclei of different sizes. All macrophage samples for measurement were photographed using a Nikon E200 optical microscope (Nikon E200, Japan; Nanjing Hengqiao Instrument Co., Ltd. C630, China). The captured images were subsequently analyzed using Image J software [33] to ensure the accuracy and reliability of the results.

Acquisition of chest CT

A 64-slice spiral CT scanner (GE Healthcare OPTIMA CT660, USA) was uesd to conduct chest CT scans on subjects in the supine position. The scans were performed during full inspiration and breath-holding. The scanning parameters were set at: tube voltage of 120 kV, automatic tube current (mA), rotation speed of 0.6 r/s, pitch of 0.985, slice thickness of 0.625 mm, and continuous sectioning mode. The images was used a standard soft-tissue kernel for the reconstruction.

Quantitative CT analysis

The inspiratory phase thin-section CT dicom images were transferred to the A-View® artificial intelligence lung quantitative imaging software (Suzhou Suhai Information Technology Co., Ltd., China) for segmentation and quantification of pulmonary blood vessels (Fig. 1). The software uses three-dimensional quantitative algorithms to automatically complete the segmentation of pulmonary lobes and vessels [34, 35]. The percentage of low-attenuation areas (LAA%) represent the proportion of areas with attenuation less than −950Hounsfield units (HU) in the CT images. A total of four lung segmental bronchi were selected and measured as previous study [27, 36], including the right apical segment (RB1) and right basal segment (RB9), as well as the left posterior apical segment (LB1+2) and the left lateral basal segment (LB9), at their sixth- and ninth-generation walls. Pulmonary vessel extraction uses software to apply region growing and weighted minimum spanning tree algorithms (MST) with direction vector fields on a threshold of -750HU to further refine the extracted initial blood vessels into a pulmonary blood vessel tree [37]. Once the pulmonary vascular tree structure was reconstructed, the lung surface areas at depths of 6 mm, 12 mm, 18 mm, and 24 mm from the pleural surface(LSA_{6mm}、LSA_{12mm}、LSA_{18mm}、LSA_{24mm}) were calculated. The total number of pulmonary vessels at different depths from the pleural surface and the number of small pulmonary vessels with a cross-section less than $5mm^2$ were counted as the original value (N_{total}; $N_{<5mm}{}^2$).For unit lung surface area at each level, N_{total} and $N_{<5mm}{}^2$ were counted as robust values and reported as the number of vessels per $1cm^2$ of lung surface area (N_{total}/ LSA ; $N_{<5mm}{}^2$/LSA) [35]. The total blood vessel volume (TBV) was determined as the total volume of the intraparenchymal pulmonary vasculature in the lungs. TBV was calculated, and the volumes of small pulmonary vessels with a cross-section area of 0-$2mm^2$ and 2-$5mm^2$(BV_{0-2}, BV_{2-5})were also calculated. The small pulmonary vessel volume fractions (BV_{0-2}/TBV and BV_{2-5}/TBV) were also calculated [19, 38, 39].Vascular volume refers to the measured volume of all arteries and veins, including the blood within the vessel wall and lumen.

Spirometry

According to the ATS/ERS Pulmonary Function Measurement Standards [40], two certified technicians used a portable calibrated electronic spirometer (CHEST-GRAPHHI-701, Japan) to measure spirometry. Each subject performed pulmonary function three times, and the best data was recorded.

Rats exposed to DE

A total of 7-week-old Sprague-Dawley male rats were purchased from Jinan Pengyue Animal Experiment Ltd. (Shandong, China) and randomly divided into the DE group ($n=6$) and the Air group ($n=6$). After one week of environmental adaptation, the DE group started receiving DE exposure in the 8th week. This involved a daily exposure of 2 h, with 1 h in the morning and 1 h in the afternoon, 5 days per week for 16 weeks. In contrast, the rats in the Air group were exposed to clean air. Throughout the study, the rats were maintained in an environment with a relative humidity of 50–60%, a temperature of 24–26 °C, and a 12-hour light/dark cycle. All rats used in this study were maintained according to protocols approved by the Animal Ethics Committee of Qingdao Municipal Hospital.

A single-cylinder diesel generator with a load power of 4000KW (Yuchai Machinery Co., Ltd., Guangxi, China) was used No. 0 diesel and run at a speed of 1500 rpm to generate DE. The generated DE is diluted to a constant concentration (3 mg/m^3) through a clean air pump, a standard concentration in DE air exposure experiments [41–43]. A real-time dust monitor (CASELLA, England) and a composite gas detector (LOOBO, China) were installed in the exposure box that received DE to detect PM2.5 concentration and the concentrations of NOx, CO, and SO_2.

Hemodynamic testing

During the experiment, the rats were anesthetized with intraperitoneal injection of sodium pentobarbital (30 mg/kg) at a concentration of 3 mg/ml to ensure complete unconsciousness. The abdomen of the rat was cut open with scissors to expose the transverse septum. Next, we opened the septum transversum and pericardium and observed the heartbeat. The manometry instrument (ADINSTRUMENT PL26T04, Australia) was connected,

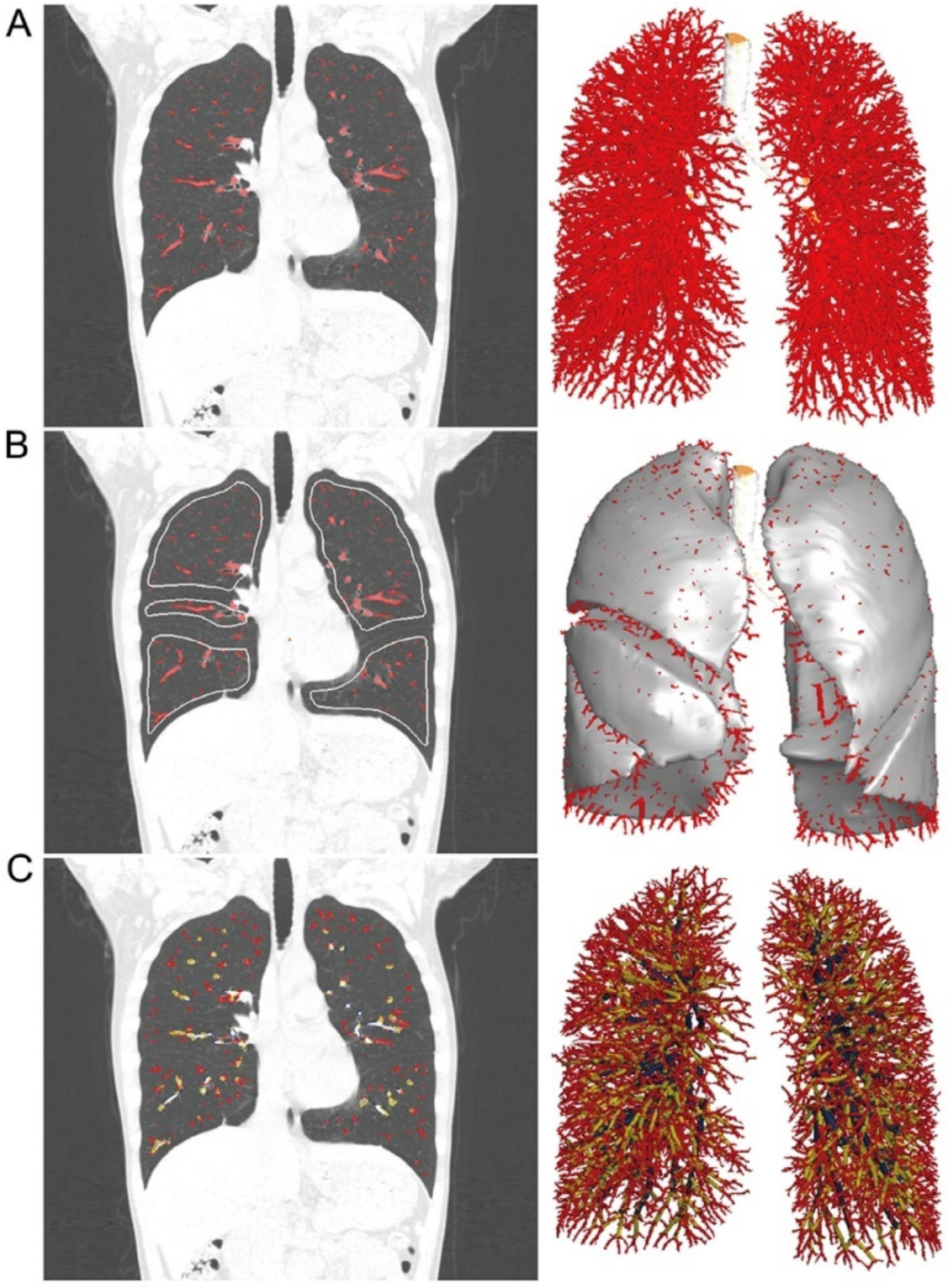

Fig. 1 Extraction and reconstruction of pulmonary vessels. (**A**) Automatic extraction and segmentation of pulmonary vessels. (**B**) Extraction and plotting of the lung surface area at different depths from the pleural surface. The white contours on the left and the white surface on the right illustrate the lung surface area 6 mm below the pleural surface. (**C**) Extraction and segmentation of the whole pulmonary vascular volume. Red represents pulmonary vessels with a cross-sectional area of 0-5mm^2; yellow represents pulmonary vessels with a cross-sectional area of 5-10mm^2; and blue represents pulmonary vessels with a cross-sectional area of 10-22mm^2

and 0.9% saline containing 100 U/ml heparin sodium was injected into the right ventricle using a 22G injection needle. The right ventricular systolic pressure (RVSP) was then detected and recorded for 30 s after stabilization, with the data being saved.

Collection and analysis of bronchoalveolar lavage fluid

After the rats were sacrificed, the chest cavity was exposed, and the left lung was ligated from the tracheal bifurcation of rats. To collect bronchoalveolar lavage fluid (BALF), the right lung was lavaged with 2 ml of PBS solution for three times. BALF was centrifuged at 700 g for 10 min, and the cell pellet and supernatant were separated. The cell pellet was resuspended in 1 ml of PBS solution, and a portion of the cell suspension was pipetted into a hemocytometer to count the total cells. Based on the counting results, a cell suspension containing a total number of 50,000 cells was drawn for Swiss-Giemsa staining. The supernatant of BALF is recovered and divided into packages for further inspection.

Histological sections and pathological scoring

Uninflated rat left lung tissue was fixed in a 4% paraformaldehyde PBS solution for 48 h. Subsequently, the lung tissue was dehydrated, embedded in paraffin, and sliced into 3 μm sections using a rotary microtome. Hematoxylin-eosin (HE) and Masson's triple staining were used to stain the lung tissue sections. The mean linear intercept (MLI), a measure of interalveolar distance, was determined as previously described [44, 45]. The blue area of collagen deposition around the pulmonary arterioles and small airways in the lung tissue sections were evaluated and scored using Image J [43, 46, 47]. Additionally, the percentage of wall thickness of pulmonary arterioles was calculated using the formula WT%=(outer diameter-inner diameter)/outer diameter*100%. For each lung section, at least 10 areas were assessed, and the average of all area scores or WT% was determined for each rat.

ELISA

The expression of macrophage migration inhibitory factor (MIF) (Elabscience E-EL-R0608, China) in BALF of rats were detected by double antibody sandwich ELISA according to the manufacturer's instructions. The minimum detectable dose of rat MIF was typically less than 1.563 ng/ml.

Table 1 Primers of RNAs for RT-PCR

Target	Forward (5′-3′)	Reverse (5′-3′)
MIF	CGGACCGGGTCTACATCAACT	AACAGCGGTGC AGGTAAGTGAG
β-actin	TCCTGTGGCATCCATGAAACT	GAAGCATTTGC GGTGCACGAT

RT-PCR

Total RNA of rat lung was extracted by Trizol (Takara, Japan). And the concentrations of isolated total RNA were determined using a spectrophotometer (NanoDrop Technologies, Wilmington, DE, USA) at 260 nm. The first strand cDNA synthesis (Reverse Transcription Kit, AG, China) and real-time PCR (SYBR® Green Pro Taq HS, AG, China) were also performed according to the manufacturer's instructions. The primer sequences of target RNAs were shown in Table 1. All the data were normalized to the housekeeping gene, β-actin. The relative RNA levels were calculated using $2^{-\triangle\triangle CT}$ method.

Statistical analysis

All the statistical analyses were conducted using IBM SPSS Statistics software (version 26.0: IBM Corp, Armonk NY). Categorical data were presented as percentages (%), and chi-square test was used for intergroup comparison. As for continuous data, the Shapiro-Wilk test was used to test normality. Normally distributed continuous data were presented as Mean ± SD, with the Student t-test used for intergroup comparison; the continuous data that did not conform to a normal distribution were expressed as medians, first and third quartiles, with the Mann-Whitney U test used for intergroup comparison. Multiple linear regression was used to assess the differences in spirometry between non-DETs and DETs after adjustment for age, BMI, smoking status and packyears. Using Generalized linear model to assess the differences in the parameters of pulmonary vessels detected by CT between non-DETs and DETs after adjustment for age, BMI, smoking status and packyears. Multiple linear regression models were conducted to explore the dose–response relationships of the CCAM levels with the number and volume of pulmonary vessels, with participants equally divided into four groups according to CCAM levels. Pearson correlation coefficients were used to assess the relation between 6th wall area percent and 9th wall area percent with the number and volume of pulmonary vessels.

Results

Exposure assessment

More than 84.3% DE particles had aerodynamic diameter less than 100 nm with 100% particles less than 1000 nm [30]. Geometric mean of PM2.5 level in the DET workshops was 430.8 μg/m^3, which was significantly higher than the level in the local water company (130.0 μg/m^3, Table 2). PM2.5 exposure of the local water company was $PM_{2.5}$ levels calculated from five air samples collected from the local water company areas in October 2018. These values were used to represent the background particulate matter levels of this study and were similar to what was reported for Luoyang city in the national

Table 2 Demographics characteristics, particulate matter exposures and spirometry of the two groups

Variable	DET group (*n* = 78)	Non-DET group (*n* = 66)	*P*
Demographics			
Age (yr, M ± SD)	36.7 ± 8.4	38.0 ± 10.4	0.384[a]
Male sex (n, %)	78,100	66,100	
Height (cm, M ± SD)	172.9 ± 4.9	176.1 ± 5.9	0.666[a]
Weight (kg, M ± SD)	75.0 ± 11.2	79.9 ± 14.3	0.671[a]
BMI (kg/m2, M ± SD)	25.8 ± 3.3	25.8 ± 4.4	0.886[a]
Smoking Status			0.486[b]
Never smoker (n, %)	18, 23.1	20, 30.3	
Current smoker (n, %)	49, 62.8	36, 54.5	
Former smoker (n, %)	11, 14.1	10, 15.1	
Packyears in ever smokers (Mdn, Q1 - Q3)	9.8, 2.6–13.2	19.4, 11.4–20.1	0.340[c]
Particulate matter exposure			
DE exposure history (yr, M ± SD)	11.5 ± 6.4	—	
$PM_{2.5}$ (μg/m3, n, GSM, GSD)	4, 430.8, 2.3	5, 130.0, 1.2	
CCAM (%, n, Mdn, Q1 - Q3)	52, 4.31, 3.00–8.00	41, 1.54, 1.20-2.00	<0.001[c]
Radiography			
LAA (%,Mdn, Q1-Q3)	0.217, 0.115–0.526	0.302, 0.120–0.597	0.837[d]
Total lung capacity (cc, M ± SD)	4877.5 ± 1239.9	5071.1 ± 1064.5	0.341[d]
Spirometry			
FEV_1 (L/s, M ± SD)	3.53 ± 0.44	3.64 ± 0.56	0.045[d]
FEV_1% predicted (%, M ± SD)	94.56 ± 11.45	98.61 ± 11.04	0.046[d]
FVC (L, M ± SD)	4.04 ± 0.54	4.16 ± 0.61	0.047[d]
FVC % predicted (%, M ± SD)	99.26 ± 11.44	101.56 ± 12.87	0.149[d]
FEV_1/FVC (%, M ± SD)	87.43 ± 5.17	87.49 ± 5.59	0.879[d]
MMF (L/s, M ± SD)	4.16 ± 0.87	4.23 ± 1.06	0.481[d]
MMF % predicted (%, M ± SD)	88.35 ± 21.37	92.74 ± 21.10	0.393[d]
FEF_{25} (L/s, M ± SD)	6.76 ± 1.18	7.19 ± 1.43	0.040[d]
FEF_{25} percent predicted (%, M ± SD)	83.07 ± 15.14	88.45 ± 17.97	0.064[d]
FEF_{50} (L/s, M ± SD)	4.74 ± 1.03	4.93 ± 1.35	0.269[d]
FEF_{50} percent predicted (%, M ± SD)	82.91 ± 19.01	87.68 ± 22.42	0.240[d]
FEF_{75} (L/s, M ± SD)	2.17 ± 0.69	2.20 ± 0.78	0.625[d]
FEF_{75} percent predicted (%, M ± SD)	75.67 ± 26.25	79.6 ± 26.01	0.605[d]

BMI: body mass index, CCAM: carbon content in airway macrophage, DET: diesel engine tester, FEV_1: forced expiratory volume in 1s, FEF_{25}: Forced expiratory flow rate at 25% vital capacity, FEF_{50}: Forced expiratory flow rate at 50% vital capacity, FEF_{75}: Forced expiratory flow rate at 75% vital capacity, FVC: forced vital capacity, GSD: geometric standard deviation; GSM: geometrical mean, L/S: liters per second, M: mean, Mdn: median, MMF: maximal mid-expiratory flow, $PM_{2.5}$: fine particulate matter, Q_1: lower quartile, Q_3: upper quartile, SD: standard deviation

[a] Student t-test

[b] Chi-square test

[c] Wilcoxon rank sum test

[d] Multiple linear regression assessed the differences in spirometry between non-DETs and DETs after adjustment for age, BMI, smoking status and packyears

air quality surveillance system of China during the same period. CCAM in DETs was significantly higher than that seen in non-DETs (Table 2).

Participant characteristics

A total of 66 healthy controls (the non-DET group) and 78 diesel engine testers (the DET group) were finally included in the data analysis of the DET cohort in 2018. All subjects were male to exclude the possible confounding influence of gender. As shown in Table 2, the median DE exposure history in the DET group was 11.5 years, and there were no significant differences in age, height, weight, and smoking status between the two groups. Compared with the non-DET group, the DET group showed decreases in forced expiratory volume in 1 s (FEV_1), forced vital capacity (FVC), and forced expiratory flow rate at 25% vital capacity (FEF_{25}).

CT imaging of airway and vessels

Our CT images showed that there was no significant difference in total lung capacity and LAA% between the DET group and the non-DET group (Table 2). Noteworthily, the DET group had significantly increased numbers of all pulmonary vessels and small pulmonary vessels

with a cross-sectional area of $<5mm^2$ at different depths from the pleural surface, compared with the non-DET group (Fig. 2A). In addition, these increasing trends were further confirmed by the robust value expressed as the number of pulmonary vessels per unit lung surface area at the same depth (N/LSA). (Fig. 2B). However, there were no difference in the diameter of large blood vessels (including ascending aorta, main pulmonary artery, left pulmonary artery and right pulmonary artery) between the DET group and non-DET group (Supplement Table 1).

Considering the more distinct differences in small pulmonary vessels with a cross-sectional area of less than $5mm^2$, we further divided them into those with a cross-sectional area of 0-$2mm^2$ and those with a cross-sectional area of 2-$5mm^2$, to investigate the relationship between DE exposure and volume of small pulmonary vessels. Compared to the non-DETs, the TBV in DETs were increased 14.7 cc (P=0.028) (Supplementary Table 1). Moreover, compared with the control group, the BV0-2 and BV0-5 in the DET group were increased 6.5 cc and 5.9 cc respectively(P<0.001, P=0.017) (Fig. 2C).These findings demonstrate that DE exposure primarily leads to an increase in TBV by augmenting the volume of small pulmonary vessels. Additionally, the small pulmonary vessel volume fractions (BV_{0-2}/TBV, BV_{2-5}/TBV) in the DET group were significantly higher than those in the non-DET group (Fig. 2D).

Generalized linear model assessed the differences in the parameters of pulmonary vessels detected by CT between non-DETs and DETs after adjustment for age, BMI, smoking status and packyears.

BV_{0-2}: Volume of small pulmonary vessels with a cross-section area of 0-$2mm^2$, BV_{2-5}: Volume of small pulmonary vessels with a cross-section area of 2-$5mm^2$, DET: diesel engine tester, LSA_{6mm}: Lung surface area at 6 mm depth from the pleural surface, LSA_{12mm}: Lung surface area at 12 mm depth from the pleural surface, LSA_{18mm}: Lung surface area at 18 mm depth from the pleural surface, LSA_{24mm}: Lung surface area at 24 mm depth from the pleural surface, $N_{total-6\ mm}$: Total number of pulmonary vessels at 6 mm depth from the pleural surface, $N_{<5mm^2-6\ mm}$: Total number of pulmonary vessels with cross-section area less than 5 mm^2 at 6 mm depth

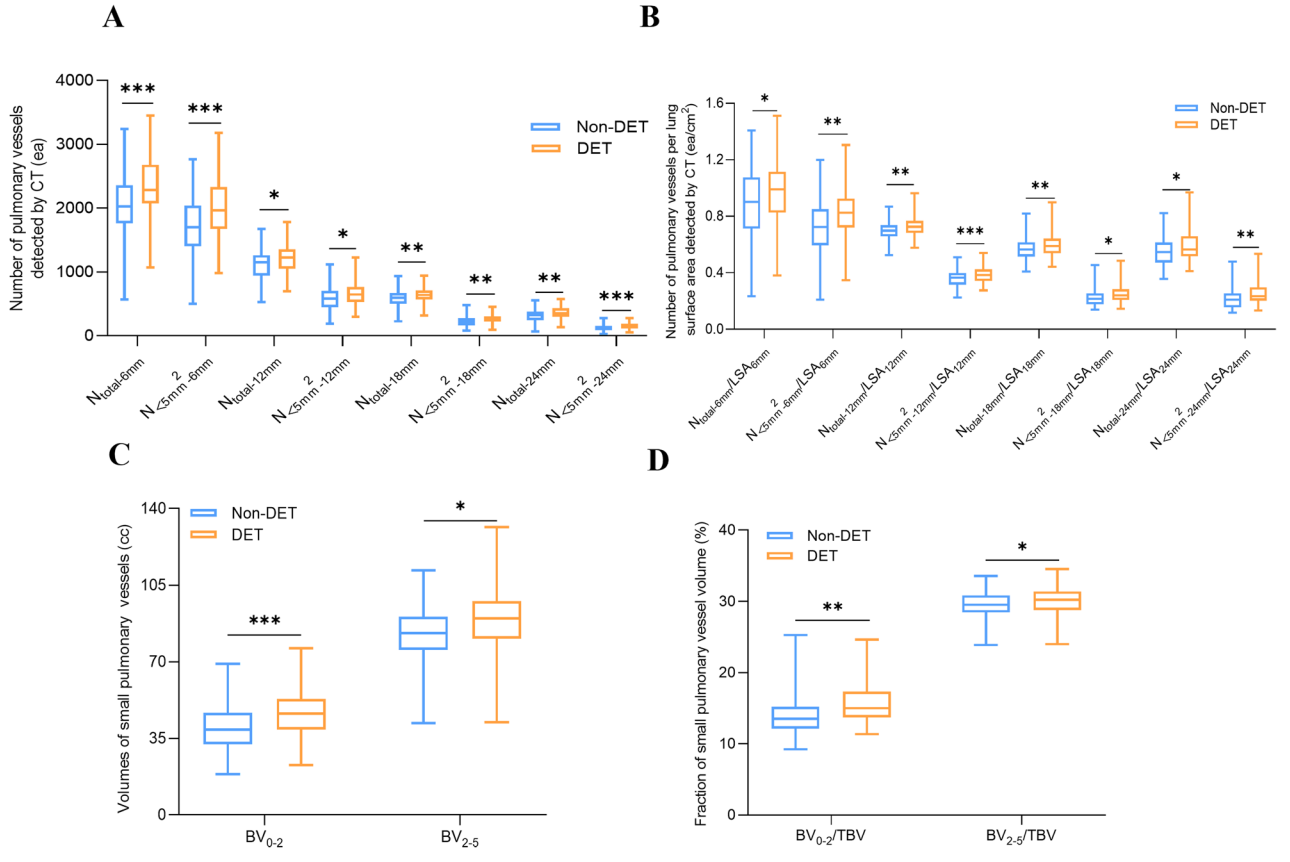

Fig. 2 Comparing the imaging parameters of small pulmonary vessels between non-DETs and DETs. (**A**) The numbers of pulmonary vessels at different depths from the pleural surface in the two groups. (**B**) The numbers of blood vessels per unit lung surface area at different subpleural depths in the two groups. (**C**) The volumes of small pulmonary vessels with a cross-section area of 0-$2mm^2$ and 2-$5mm^2$ (BV_{0-2} and BV_{2-5}) in the two groups. (**D**) The small pulmonary vessel volume fractions in two groups. * $p<0.05$,** $p<0.01$, *** $p<0.001$

from the pleural surface, $N_{total-12\ mm}$: Total number of pulmonary vessels at 12 mm depth from the pleural surface, $N_{<5mm^2-12\ mm}$: Total number of pulmonary vessels with a cross-section area of less than 5 mm^2 at 12 mm depth from the pleural surface, $N_{total-18\ mm}$: Total number of pulmonary vessels at 18 mm depth from the pleural surface, $N_{<5mm^2-18\ mm}$: Total number of pulmonary vessels with a cross-section area of less than 5 mm^2 at 18 mm depth from the pleural surface, $N_{total-24\ mm}$: Total number of pulmonary vessels at 24 mm depth from the pleural surface, $N_{<5mm^2-24\ mm}$: Total number of pulmonary vessels with a cross-section area of less than 5 mm^2 at 24 mm depth from the pleural surface, TBV: Total blood vessel volume.

The dose–response relationships of CCAM with the number and volume of pulmonary vessels

A total of 41 non-DETs and 52 DETs with analyzable CT scans and available CCAM data were included in our correlation analyses. They were divided equally into 4 groups (Group 1,2,3,4) based on CCAM levels. Using the first CCAM group (0.46–1.54) as the reference, we found that all the other three groups had greater numbers of pulmonary vessels at various subpleural depths, while only the fourth CCAM group (≥4.7%) showed significant differences (all $P<0.05$) (Table 3). However, the overall trend test showed there were significant increasing trends in the numbers of pulmonary vessels at various subpleural depths with the increase of CCAM levels (all P for trend < 0.05). Moreover, the number of small pulmonary vessels per unit lung surface area at various subpleural depths also showed an increasing trend with increasing CCAM levels (Table 3). Increased CCAM was observed to have stronger dose-dependent relationships with BV_{0-2} and BV_{0-2}/TBV (Table 4). To be specific, the third and fourth CCAM groups showed significant differences in BV_{0-2} and BV_{0-2}/TBV, compared to the reference group. The overall trend test showed that there were stronger increasing overall trends in BV_{0-2} and BV_{0-2}/TBV with the increase of CCAM levels.

Correlations between pulmonary small airway parameters and pulmonary vascular parameters in CT

In previous study, we found that the increased wall area percentage (WA%) of 6th and 9th bronchi served as an indicator of early airway damage due to DE exposure (Liu et al., 2021). To investigate the potential association with airway and pulmonary vascular damage, the average WA% of the bronchus LB1+2, LB9, RB1, and RB9 was measured and assessed in relation to the number and volume of small pulmonary vessels. However, there is no significant correlation between WA% (6th and 9th) and the number and volume of pulmonary vessels (Supplementary Table 3), which suggesting that airway remodeling and pulmonary vessel remodeling are independent.

Cardiopulmonary vascular remodeling

To further investigate the potential impact of chronic exposure to DE on pulmonary vasculature and airways, we constructed a chronic DE-exposed rat model. Our findings from the rat model indicated increased accumulation of diesel exhaust particles in macrophages in the BALF of rats in the DE group (Fig. 3A). Histopathological evaluation revealed that rats in the DE group exhibited larger mean linear intercept (MLI) of the alveoli (Supplementary Fig. 1A and B) and heightened collagen deposition around the small airway compared to the control group (Supplementary Fig. 1C and D). In addition, the percentage of small pulmonary vessel wall thickness (WT%) was significantly higher (Fig. 3B), and collagen deposition around small pulmonary vessels was increased in the DE group (Fig. 3C). Furthermore, hemodynamic results demonstrated that rats in the DE group had increased right ventricular intraventricular pressure (RVSP) and right ventricular hypertrophy index (RVHI) compared to the control group (Fig. 3D E). Therefore, the proliferation of smooth muscle maybe the principal basis of the increase in the number and volume of pulmonary small vessels in DETs.

The expression of macrophage migration inhibitory factor (MIF)

MIF was increased in BALF and lung tissues in the DE group (Fig. 3F G). A combination of the above elevated parameters are indicative of the remodeling of small pulmonary vessels and cardiac remodeling in DE-exposed rats, suggesting that DE exposure might lead to the remodeling of pulmonary vessels and cardiac structures as well as the subsequent decline of right heart function through promoting the expression of MIF.

Discussion

This is the first study to use artificial intelligence quantitative lung imaging software to assess the effects of DE exposure on pulmonary vessels. In this study, we analyzed the pulmonary vessels in chest CT of subjects with occupational DE exposure and histopathological changes in chronic DE-exposed rats, which indicating that long-term exposure to DE might lead to the remodeling of small pulmonary vessels through promoting the expression of MIF.

As the most popular traffic pollutant, DE has brought profound health effects on airway inflammation and remodeling, however, there is limited research on the pulmonary vascular effects. In this study, we employed the A-View® artificial intelligence platform to analyze

Table 3 The dose-response relationships between CCAM and the number of pulmonary vessels at various subpleural depths in all the study participants ($n=93$) [a]

Parameters of pulmonary vessel number detected by CT	CCAM		*N*	M ± SD	*P* value
	Category	Range (%)	DET		
$N_{total-6\ mm}$, ea	1	0.46–1.54	24(3)	1953.54 ± 431.79	
	2	1.54–3.10	23(11)	2091.48 ± 503.43	0.402
	3	3.10–4.70	23(17)	2163.48 ± 510.31	0.272
	4	4.70-30.24	23(21)	2330.48 ± 598.94	0.008
Trend test [b]					0.008
$N_{total-12\ mm}$, ea	1	0.46–1.54	24(3)	1041.54 ± 257.26	
	2	1.54–3.10	23(11)	1091.00 ± 199.06	0.729
	3	3.10–4.70	23(17)	1119.30 ± 207.81	0.644
	4	4.70-30.24	23(21)	1212.52 ± 212.62	0.044
Trend test [b]					0.049
$N_{total-18\ mm}$, ea	1	0.46–1.54	24(3)	536.75 ± 146.69	
	2	1.54–3.10	23(11)	605.74 ± 123.31	0.148
	3	3.10–4.70	23(17)	607.22 ± 130.78	0.243
	4	4.70-30.24	23(21)	636.91 ± 124.24	0.037
Trend test [b]					0.049
$N_{total-24\ mm}$, ea	1	0.46–1.54	24(3)	279.38 ± 103.92	
	2	1.54–3.10	23(11)	335.43 ± 88.73	0.116
	3	3.10–4.70	23(17)	332.00 ± 94.81	0.220
	4	4.70-30.24	23(21)	358.35 ± 81.61	0.024
Trend test [b]					0.043
$N_{<5mm^2-6\ mm}$, ea	1	0.46–1.54	24(3)	1579.21 ± 428.00	
	2	1.54–3.10	23(11)	1749.74 ± 490.08	0.354
	3	3.10–4.70	23(17)	1783.17 ± 457.75	0.328
	4	4.70-30.24	23(21)	2009.78 ± 551.68	0.004
Trend test [b]					0.005
$N_{<5mm^2-12\ mm}$, ea	1	0.46–1.54	24(3)	508.04 ± 257.26	
	2	1.54–3.10	23(11)	544.09 ± 151.39	0.830
	3	3.10–4.70	23(17)	584.52 ± 147.32	0.397
	4	4.70-30.24	23(21)	672.26 ± 184.88	0.016
Trend test [b]					0.011
$N_{<5mm^2-18\ mm}$, ea	1	0.46–1.54	24(3)	199.50 ± 63.23	
	2	1.54–3.10	23(11)	234.13 ± 62.61	0.088
	3	3.10–4.70	23(17)	261.74 ± 69.67	0.010
	4	4.70-30.24	23(21)	273.35 ± 72.77	0.001
Trend test [b]					0.001
$N_{<5mm^2-24\ mm}$, ea	1	0.46–1.54	24(3)	107.63 ± 45.52	
	2	1.54–3.10	23(11)	137.35 ± 45.81	0.057
	3	3.10–4.70	23(17)	146.00 ± 52.01	0.026
	4	4.70-30.24	23(21)	152.61 ± 45.21	0.003
Trend test [b]					0.004
$N_{<5mm^2-6\ mm}/LSA_{6mm}$, ea/cm^2	1	0.46–1.54	24(3)	0.72 ± 0.15	
	2	1.54–3.10	23(11)	0.74 ± 0.18	0.671
	3	3.10–4.70	23(17)	0.76 ± 0.17	0.405
	4	4.70-30.24	23(21)	0.80 ± 0.20	0.038
Trend test [b]					0.033
$N_{<5mm^2-12\ mm}/LSA_{12mm}$, ea/cm^2	1	0.46–1.54	24(3)	0.34 ± 0.06	
	2	1.54–3.10	23(11)	0.34 ± 0.05	0.555
	3	3.10–4.70	23(17)	0.37 ± 0.05	0.212
	4	4.70-30.24	23(21)	0.40 ± 0.05	0.005
Trend test [b]					0.001
$N_{<5mm^2-18\ mm}/LSA_{18mm}$, ea/cm^2	1	0.46–1.54	24(3)	0.23 ± 0.07	

Table 3 (continued)

Parameters of pulmonary vessel number detected by CT	CCAM		*N*	M ± SD	*P* value
	Category	Range (%)	DET		
	2	1.54–3.10	23(11)	0.23 ± 0.05	0.583
	3	3.10–4.70	23(17)	0.26 ± 0.07	0.035
	4	4.70-30.24	23(21)	0.25 ± 0.05	0.065
Trend test [b]					0.021
$N_{<5mm^2-24\,mm}/LSA_{24mm}$, ea/cm^2	1	0.46–1.54	24(3)	0.23 ± 0.08	
	2	1.54–3.10	23(11)	0.24 ± 0.06	0.388
	3	3.10–4.70	23(17)	0.27 ± 0.09	0.032
	4	4.70-30.24	23(21)	0.25 ± 0.07	0.120
Trend test [b]					0.055

CCAM: carbon content in airway macrophage, DET: diesel engine tester, M: mean, SD: standard deviation, other abbreviations are the same as those in Fig. 2

[a] Multiple linear regression assessed differences of number of pulmonary vessels at different subpleural depths between categories 2–4 and the reference group (category 1) with adjustment of age, BMI and smoking status and packyears

[b] Multiple linear regression assessed the dose–response relationships between CCAM category coded as 1, 2, 3 and 4 and number of pulmonary vessels at different subpleural depths with adjustment for covariates listed above

Table 4 The dose-response relationship between CCAM and the volume of small pulmonary vessels in all the study participants ($n = 93$) [a]

Parameters of pulmonary vessel volume detected by CT	CCAM		*N*	M ± SD	*P* value
	Category	Range (%)	DET		
$BV_{0-2,}$ cc	1	0.46–1.54	24(3)	37.01 ± 10.36	
	2	1.54–3.10	23(11)	42.01 ± 7.63	0.099
	3	3.10–4.70	23(17)	45.47 ± 10.51	0.012
	4	4.70-30.24	23(21)	46.82 ± 12.48	0.001
Trend test [b]					0.001
BV_{0-2}/TBV, %	1	0.46–1.54	24(3)	12.38 ± 2.78	
	2	1.54–3.10	23(11)	14.44 ± 1.37	0.136
	3	3.10–4.70	23(17)	15.66 ± 2.21	0.003
	4	4.70-30.24	23(21)	16.09 ± 3.32	<0.001
Trend test [b]					<0.001

CCAM: carbon content in airway macrophage, DET: diesel engine tester, SD: standard deviation, other abbreviations as in Fig. 2

[a] Multiple linear regression assessed the differences in the volume of small pulmonary vessels between categories 2–4 and the reference group (category 1) with adjustment of age, BMI, and smoking status and packyears

[b] Multiple linear regression assessed dose – response relation between CCAM category coded as 1, 2, 3 and 4 and volume of small pulmonary vessel with adjustment for covariates listed above

the CT images of the occupational DE exposed populations. As results, all subjects had no obvious percentage of low-attenuation areas detected by CT and no spirometry diagnosis of airway obstruction. More small vessels were captured by CT in the DETs group due to proliferation and hypertrophy of smooth muscle cells in small vessels, as well as higher volumes of small pulmonary vessels compare to the control members [48, 49]. Consistent to this results, several cohort studies associated with traffic pollution, such as ozone [50], black carbon [51], also shown increased pulmonary vascular resistance and adverse effect on the number of pulmonary vessels. Furthermore, there are positive correlation between amount of DE exposure and some imaging parameters of small pulmonary vessels, in a cross-sectional area of 0–2 mm^2, not in 2-5mm^2(Supplementary Table 2). To be noticed, since most pulmonary artery remodeling started from small pulmonary vessels, this remodeling is asymptomatic until the pulmonary hypertension occur with enormous lost (roughly 50–70%) of the pulmonary vascular bed due to emphysema or other reasons [52].

In previous study, we had shown that DE exposure can lead to small airway wall thickening without lumen stenosis, occurring before airflow limitation [27]. Here we demonstrated that small airway remodeling was not directly linked to small pulmonary vessel remodeling due to DE exposure. Consistent with this, pulmonary vascular dysfunction and remodeling have been observed before airflow limitation in cigarette smoke animal or smokers [53, 54]. Therefore, the lung health effects of DE exposure are all from distal portion of airway or pulmonary vessels.

To reveal the mechanisms of the vessel remodeling of DE exposure, we conduct a chronic DE exposure animal experiment. Our study showed that DE-exposed rats had increased thickness of the small pulmonary vessels, larger mean linear intercept of the alveoli, more

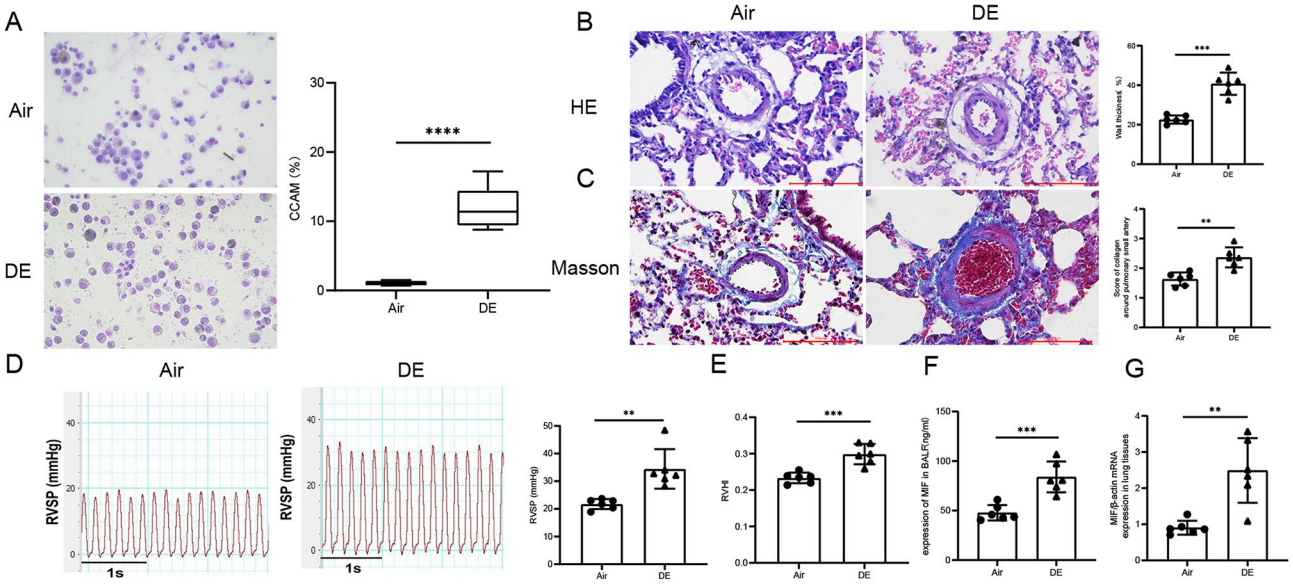

Fig. 3 Effect of DE exposure on rat pulmonary artery pressure and pulmonary vessels. (**A**) CCAM in BALF in rats. (**B**) HE staining to assess small pulmonary vessel wall thickness in rats. (**C**) Masson staining to assess collagen deposition around rat small pulmonary vessels in rats. (**D**) Hemodynamic conditions of rats between the two groups. (**E**) RVHI of rats between the two groups. (**F**) MIF expression in BALF between the two groups. (**G**) MIF expression in lung tissues between the two groups. Data were presented as means ± SD ($n = 6$). ** $p < 0.01$, *** $p<0.001$, ****$P<0.0001$; scale bar = 100 μm; BALF: bronchoalveolar lavage fluid; DE: diesel exhaust; RVSP: right ventricular systolic pressure; RVHI: right ventricular hypertrophy index

collagen deposition around the small pulmonary vessels and small airways, and higher RVSP (Fig. 3 and Supplemental Fig. 1). Of course, this DE exposure concentration ($3mg/m^3$) is notably higher than the 430.8ug/m3 DETs concentration in the workshop, may explain the rapid appearance of airway and pulmonary vessel changes in the animal model. Consistent with our results, Davel et al. reported that environmental particulate exposure has led to continuous contracted small pulmonary vessels with increase of endothelin [55], and Liu et al. demonstrated the thickening of pulmonary artery wall, as well as apoptosis of vascular endothelial cells and proliferation of vascular smooth muscle cells [48]. However, the mechanisms of DE exposure on vascular remodeling have not been clarified yet.

As a pro-inflammatory and pro-proliferative factor, MIF was secreted by various cell types, including epithelial cells, T cells, macrophages, as well as impaired the airway epithelial and smooth muscle cells [56]. In our experiments, MIF in both the lung tissue and BALF was increased in the DE rats. In turn, MIF can recruit and activate a substantial number of alveolar macrophages and pulmonary interstitial macrophages and then resulting the release of various inflammatory mediators (such as TNF-a, IL-6) and angiogenic factors (such as PDGF, VEGF), which play a crucial role in the development of pulmonary vascular remodeling [57].

The A-view system utilized in this study offers fully automatic analysis and segmentation of pulmonary vessels, and can analysis through low-dose CT scans [21]. In comparison to the initial chest imaging platform created by the Applied Chest Imaging Laboratory of Brigham and Women's Hospital [19, 50], this system has the advanced ability to identify smaller pulmonary vessels [21], potentially allowing for earlier detection of individuals exhibiting indicative of pulmonary vascular dysfunction. Furthermore, the Apollo automated lung quantification system by VIDA requires contrast media injection for detecting smaller pulmonary vessels [58, 59], posing challenges for patients with renal insufficiency or critically ill patients. Besides utilizing small pulmonary vessel volume as an assessment metric, this system has introduced a novel indicator, the number of blood vessels, as a diagnostic criterion, offering a new approach to evaluating small pulmonary vessels.

To be honestly, there are still certain limitations for pulmonary vascular analysis by A-view system. Firstly, it is unable to differentiate between small pulmonary arteries and veins without contrast media. Secondly, due to the similarity in tissue density between blood vessel walls and blood on CT, it cannot measure the thickness of small blood vessel walls or the extent of luminal stenosis. Further research should be carried out to improve the resolution and sensitivity of CT scan or new detective methods.

Conclusions

In this study, DE exposure contributed to the increases in the number and volume of peripheral small pulmonary vessels, which possible through enhancing the expression

and secretion of MIF, ultimately resulting in the formation of pulmonary hypertension.

Supplementary Information

The online version contains supplementary material available at https://doi.org/10.1186/s12931-024-02976-y.

Supplementary Material 1

Supplementary Material 2

Supplementary Material 3

Supplementary Material 4

Acknowledgements

1. This study is very grateful to Suhai Co., Ltd., Suzhou China for technical assistance in the analyze of A-view system.
2. The biggest advantage of this study is that the exposed subjects came from a DET cohort in Henan, the diesel engine tester cohort, and the environmental particulate matter has been comprehensively described in previous studies and environmental assessments [27, 30]. Compared with other diesel exhaust cohorts [60–62], this cohort does not have the impact of other co-exposure confounding factors (such as mine dust, coal, silica, etc.).

Author contributions

Chaohui M.wrote the main manuscript text, acquired and analysised the data; Qinghai L. Niu Y.substantively revised the manuscript; Yinjuan Y. Ting H. analysised and interpreted the data; Yanting L. Tao w. Yiqiao L. Huiling T.Jing J. Haibin X acquired the data; Wei H. Yuxin Z.design the work, Provide financial support and substantively revised the manuscript.

Funding

This work was supported by the National Natural Science Foundation of China (grant No. 81973012 and grant No. 82470018), and Science and technology development plan program of Shinan district of Qingdao (2022-4-002-YY).

Data availability

No datasets were generated or analysed during the current study.

Declarations

Ethical approval

Written informed consent was acquired from all participants prior to the interview and any procedures. The protocol was approved by the Medical Ethical Review Committee of the National Institute for Occupational Health and Poison Control, Chinese Center for Disease Control and Prevention The animal experimental protocols were approved by the Animal Care and Use Committee of Qingdao University and confirmed to the Guide for the Care and Use of Laboratory Animals.

Consent for publication

Not Applicable.

Competing interests

The authors declare no competing interests.

Author details

[1]Department of Pulmonary and Critical Care Medicine, Qingdao Municipal Hospital, School of Medicine, Qingdao University, Qingdao 266071, China
[2]Qingdao Key Lab for Common Diseases, Qingdao Hospital, University of Rehabilitation and Health Sciences, Qingdao 266071, China
[3]School of Public Health, Qingdao University, Qingdao 266071, China
[4]National Institute of Occupational Health and Posing Control, China CDC, Beijing 100050, China
[5]Department of Pulmonary and Critical Care Medicine, Qingdao Hospital, Dalian Medical University, Dalian 116000, China
[6]Department of Ultrasound, Qingdao Hospital, University of Rehabilitation and Health Sciences, Qingdao 266071, China
[7]Department of Radiology, Qingdao Hospital, University of Rehabilitation and Health Sciences, Qingdao 266071, China

Received: 22 May 2024 / Accepted: 10 September 2024
Published online: 28 September 2024

References

1. Ilar A, Plato N, Lewné M, Pershagen G, Gustavsson P. Occupational exposure to diesel motor exhaust and risk of lung cancer by histological subtype: a population-based case-control study in Swedish men. Eur J Epidemiol. 2017;32:711–9.
2. Wang D-y, Cao J-h, Tan P-q, Wang Z-x, Li W-l, Liu Z-w, Wang J. Full course evolution characteristics of DPF active regeneration under different inlet HC concentrations. Fuel. 2022;310:122452.
3. Breton CV, Salam MT, Wang X, Byun HM, Siegmund KD, Gilliland FD. Particulate matter, DNA methylation in nitric oxide synthase, and childhood respiratory disease. Environ Health Perspect. 2012;120:1320–6.
4. Ogrizek M, Kroflič A, Šala M. Critical review on the development of analytical techniques for the elemental analysis of airborne particulate matter. Trends Environ Anal Chem. 2022;33:e00155.
5. Reis H, Reis C, Sharip A, Reis W, Zhao Y, Sinclair R, Beeson L. Diesel exhaust exposure, its multi-system effects, and the effect of new technology diesel exhaust. Environ Int. 2018;114:252–65.
6. DIESEL AND GASOLINE ENGINE EXHAUSTS AND SOME NITROARENES. IARC MONOGRAPHS ON, THE EVALUATION OF CARCINOGENIC RISKS TO HUMANS. IARC Monogr Eval Carcinog Risks Hum. 2014;105:9–699.
7. Ryu MH, Afshar T, Li H, Wooding DJ, Orach J, Zhou JS, Murphy S, Lau KSK, Schwartz C, Yuen ACY, et al. Impact of exposure to Diesel Exhaust on inflammation markers and proteases in former smokers with chronic obstructive Pulmonary Disease: a Randomized, Double-blinded, crossover study. Am J Respir Crit Care Med. 2022;205:1046–52.
8. Cheng I, Yang J, Tseng C, Wu J, Shariff-Marco S, Park SL, Conroy SM, Inamdar PP, Fruin S, Larson T, et al. Traffic-related Air Pollution and Lung Cancer incidence: the California Multiethnic Cohort Study. Am J Respir Crit Care Med. 2022;206:1008–18.
9. Wauters A, Vicenzi M, De Becker B, Riga JP, Esmaeilzadeh F, Faoro V, Vachiéry JL, van de Borne P, Argacha JF. At high cardiac output, diesel exhaust exposure increases pulmonary vascular resistance and decreases distensibility of pulmonary resistive vessels. Am J Physiol Heart Circ Physiol. 2015;309:H2137–2144.
10. Aaron CP, Chervona Y, Kawut SM, Diez Roux AV, Shen M, Bluemke DA, Van Hee VC, Kaufman JD, Barr RG. Particulate matter exposure and cardiopulmonary differences in the multi-ethnic study of atherosclerosis. Environ Health Perspect. 2016;124:1166–73.
11. D'Souza JC, Kawut SM, Elkayam LR, Sheppard L, Thorne PS, Jacobs DR Jr., Bluemke DA, Lima JAC, Kaufman JD, Larson TV, Adar SD. Ambient Coarse Particulate Matter and the right ventricle: the multi-ethnic study of atherosclerosis. Environ Health Perspect. 2017;125:077019.
12. Hu T, Sun F, Yu X, Li Q, Zhao L, Hao W, Han W. CC16-TNF-α negative feedback loop formed between Clara cells and normal airway epithelial cells protects against diesel exhaust particles exposure-induced inflammation. Aging. 2021;13:19442–59.
13. Steiner S, Bisig C, Petri-Fink A, Rothen-Rutishauser B. Diesel exhaust: current knowledge of adverse effects and underlying cellular mechanisms. Arch Toxicol. 2016;90:1541–53.
14. Yue W, Tong L, Liu X, Weng X, Chen X, Wang D, Dudley SC, Weir EK, Ding W, Lu Z, et al. Short term Pm2.5 exposure caused a robust lung inflammation, vascular remodeling, and exacerbated transition from left ventricular failure to right ventricular hypertrophy. Redox Biol. 2019;22:101161.
15. Durmus N, Chen WC, Park SH, Marsh LM, Kwon S, Nolan A, Grunig G. Resistin-like Molecule α and pulmonary vascular remodeling: a Multi-strain Murine Model of Antigen and Urban Ambient Particulate Matter Co-exposure. Int J Mol Sci 2023, 24.
16. Grunig G, Marsh LM, Esmaeil N, Jackson K, Gordon T, Reibman J, Kwapiszewska G, Park SH. Perspective: ambient air pollution: inflammatory response and effects on the lung's vasculature. Pulm Circ. 2014;4:25–35.
17. Liu Q, Yang Y, Wu M, Wang M, Yang P, Zheng J, Du Z, Pang Y, Bao L, Niu Y, Zhang R. Hub gene ELK3-mediated reprogramming lipid metabolism regulates phenotypic switching of pulmonary artery smooth muscle cells to

develop pulmonary arterial hypertension induced by PM(2.5). J Hazard Mater. 2024;465:133190.
18. Shikata H, McLennan G, Hoffman EA, Sonka M. Segmentation of pulmonary vascular trees from thoracic 3D CT images. Int J Biomed Imaging. 2009;2009:636240.
19. Estépar RS, Kinney GL, Black-Shinn JL, Bowler RP, Kindlmann GL, Ross JC, Kikinis R, Han MK, Come CE, Diaz AA, et al. Computed tomographic measures of pulmonary vascular morphology in smokers and their clinical implications. Am J Respir Crit Care Med. 2013;188:231–9.
20. Cho YH, Lee SM, Seo JB, Kim N, Bae JP, Lee JS, Oh YM, Do-Lee S. Quantitative assessment of pulmonary vascular alterations in chronic obstructive lung disease: associations with pulmonary function test and survival in the KOLD cohort. Eur J Radiol. 2018;108:276–82.
21. Pu Y, Zhou X, Zhang D, Guan Y, Xia Y, Liu S, Fan L. Quantitative Assessment characteristics of small pulmonary vessel remodelling in populations at high risk for COPD and smokers using low-dose CT. Int J Chron Obstruct Pulmon Dis. 2024;19:51–62.
22. Muñoz-Esquerre M, López-Sánchez M, Escobar I, Huertas D, Penín R, Molina-Molina M, Manresa F, Dorca J, Santos S. Systemic and pulmonary vascular remodelling in Chronic Obstructive Pulmonary Disease. PLoS ONE. 2016;11:e0152987.
23. Yoshimura K, Suzuki Y, Uto T, Sato J, Imokawa S, Suda T. Morphological changes in small pulmonary vessels are associated with severe acute exacerbation in chronic obstructive pulmonary disease. Int J Chron Obstruct Pulmon Dis. 2016;11:1435–45.
24. Coste F, Dournes G, Dromer C, Blanchard E, Freund-Michel V, Girodet PO, Montaudon M, Baldacci F, Picard F, Marthan R, et al. CT evaluation of small pulmonary vessels area in patients with COPD with severe pulmonary hypertension. Thorax. 2016;71:830–7.
25. Jacob J, Bartholmai BJ, Rajagopalan S, Kokosi M, Nair A, Karwoski R, Walsh SL, Wells AU, Hansell DM. Mortality prediction in idiopathic pulmonary fibrosis: evaluation of computer-based CT analysis with conventional severity measures. Eur Respir J 2017, 49.
26. Zhang X, Duan H, Gao F, Li Y, Huang C, Niu Y, Gao W, Yu S, Zheng Y. Increased micronucleus, nucleoplasmic bridge, and nuclear bud frequencies in the peripheral blood lymphocytes of diesel engine exhaust-exposed workers. Toxicol Sci. 2015;143:408–17.
27. Liu H, Li J, Ma Q, Tang J, Jiang M, Cao X, Lin L, Kong N, Yu S, Sood A, et al. Chronic exposure to diesel exhaust may cause small airway wall thickening without lumen narrowing: a quantitative computerized tomography study in Chinese diesel engine testers. Part Fibre Toxicol. 2021;18:14.
28. Wang H, Duan H, Meng T, Yang M, Cui L, Bin P, Dai Y, Niu Y, Shen M, Zhang L, et al. Local and systemic inflammation may mediate Diesel Engine Exhaust-Induced lung function impairment in a Chinese Occupational Cohort. Toxicol Sci. 2018;162:372–82.
29. Bin P, Shen M, Li H, Sun X, Niu Y, Meng T, Yu T, Zhang X, Dai Y, Gao W, et al. Increased levels of urinary biomarkers of lipid peroxidation products among workers occupationally exposed to diesel engine exhaust. Free Radic Res. 2016;50:820–30.
30. Niu Y, Zhang X, Meng T, Wang H, Bin P, Shen M, Chen W, Yu S, Leng S, Zheng Y. Exposure characterization and estimation of benchmark dose for cancer biomarkers in an occupational cohort of diesel engine testers. J Expo Sci Environ Epidemiol. 2018;28:579–88.
31. Cheng W, Liu Y, Tang J, Duan H, Wei X, Zhang X, Yu S, Campen MJ, Han W, Rothman N, et al. Carbon content in airway macrophages and genomic instability in Chinese carbon black packers. Arch Toxicol. 2020;94:761–71.
32. Wang L, Zhang H, Sun L, Gao W, Xiong Y, Ma A, Liu X, Shen L, Li Q, Yang H. Manipulation of macrophage polarization by peptide-coated gold nanoparticles and its protective effects on acute lung injury. J Nanobiotechnol. 2020;18:38.
33. Bai Y, Brugha RE, Jacobs L, Grigg J, Nawrot TS, Nemery B. Carbon loading in airway macrophages as a biomarker for individual exposure to particulate matter air pollution - A critical review. Environ Int. 2015;74:32–41.
34. Park S, Lee SM, Kim N, Seo JB, Shin H. Automatic reconstruction of the arterial and venous trees on volumetric chest CT. Med Phys. 2013;40:071906.
35. Park SW, Lim MN, Kim WJ, Bak SH. Quantitative assessment the longitudinal changes of pulmonary vascular counts in chronic obstructive pulmonary disease. Respir Res. 2022;23:29.
36. Cao X, Lin L, Sood A, Ma Q, Zhang X, Liu Y, Liu H, Li Y, Wang T, Tang J, et al. Small Airway Wall Thickening assessed by computerized tomography is Associated with low lung function in Chinese Carbon Black Packers. Toxicol Sci. 2020;178:26–35.
37. Pompe E, Galbán CJ, Ross BD, Koenderman L, Ten Hacken NH, Postma DS, van den Berge M, de Jong PA, Lammers JJ. Mohamed Hoesein FA: Parametric response mapping on chest computed tomography associates with clinical and functional parameters in chronic obstructive pulmonary disease. Respir Med. 2017;123:48–55.
38. Synn AJ, Li W, San José Estépar R, Zhang C, Washko GR, O'Connor GT, Araki T, Hatabu H, Bankier AA, Mittleman MA, Rice MB. Radiographic pulmonary vessel volume, lung function and airways disease in the Framingham Heart Study. Eur Respir J 2019, 54.
39. Huang YS, Chen ZW, Lee WJ, Wu CK, Kuo PH, Hsu HH, Tang SY, Tsai CH, Su MY, Ko CL, et al. Treatment response evaluation by computed Tomography Pulmonary vasculature analysis in patients with chronic Thromboembolic Pulmonary Hypertension. Korean J Radiol. 2023;24:349–61.
40. Miller MR, Hankinson J, Brusasco V, Burgos F, Casaburi R, Coates A, Crapo R, Enright P, van der Grinten CP, Gustafsson P, et al. Standardisation of spirometry. Eur Respir J. 2005;26:319–38.
41. Wang N, Li Q, Liu H, Lin L, Han W, Hao W. Role of C/EBPα hypermethylation in diesel engine exhaust exposure-induced lung inflammation. Ecotoxicol Environ Saf. 2019;183:109500.
42. Saito Y, Azuma A, Kudo S, Takizawa H, Sugawara I. Long-term inhalation of diesel exhaust affects cytokine expression in murine lung tissues: comparison between low- and high-dose diesel exhaust exposure. Exp Lung Res. 2002;28:493–506.
43. Yin Y, Mu C, Wang J, Wang Y, Hu W, Zhu W, Yu X, Hao W, Zheng Y, Li Q, Han W. CXCL17 Attenuates Diesel Exhaust Emissions Exposure-Induced Lung Damage by Regulating Macrophage Function. *Toxics* 2023, 11.
44. Fang ZF, Wang ZN, Chen Z, Peng Y, Fu Y, Yang Y, Han HL, Teng YB, Zhou W, Xu D, et al. Fine particulate matter contributes to COPD-like pathophysiology: experimental evidence from rats exposed to diesel exhaust particles. Respir Res. 2024;25:14.
45. Pasupneti S, Tian W, Tu AB, Dahms P, Granucci E, Gandjeva A, Xiang M, Butcher EC, Semenza GL, Tuder RM, et al. Endothelial HIF-2α as a key endogenous mediator preventing Emphysema. Am J Respir Crit Care Med. 2020;202:983–95.
46. Gu W, Li G, Zhang W, Zhang X, He Y, Huang L, Yan Y, Ji W, Hao C, Chen Z. MiR-29b regulates Th2 cell differentiation in asthma by targeting inducible B7-H3 and STAT3. Clin Transl Allergy. 2022;12:e12114.
47. Chou HC, Chen CM. Hyperoxia induces ferroptosis and impairs Lung Development in neonatal mice. Antioxid (Basel) 2022, 11.
48. Liu J, Ye X, Ji D, Zhou X, Qiu C, Liu W, Yu L. Diesel exhaust inhalation exposure induces pulmonary arterial hypertension in mice. Environ Pollut. 2018;237:747–55.
49. Lemos M, Mohallen SV, Macchione M, Dolhnikoff M, Assunção JV, Godleski JJ, Saldiva PH. Chronic exposure to urban air pollution induces structural alterations in murine pulmonary and coronary arteries. Inhal Toxicol. 2006;18:247–53.
50. Synn AJ, Byanova KL, Li W, Gold DR, Di Q, Kloog I, Schwartz J, San José Estépar R, Washko GR, O'Connor GT, et al. Ambient air pollution exposure and radiographic pulmonary vascular volumes. Environ Epidemiol. 2021;5:e143.
51. Aaron CP, Hoffman EA, Kawut SM, Austin JHM, Budoff M, Michos ED, Hinckley Stukovsky K, Sack C, Szpiro AA, Watson KD et al. Ambient air pollution and pulmonary vascular volume on computed tomography: the MESA Air Pollution and Lung cohort studies. Eur Respir J 2019, 53.
52. Austin ED, Kawut SM, Gladwin MT, Abman SH. Pulmonary hypertension: NHLBI Workshop on the primary Prevention of Chronic Lung diseases. Ann Am Thorac Soc. 2014;11(Suppl 3):S178–185.
53. Huertas A, Guignabert C, Barberà JA, Bärtsch P, Bhattacharya J, Bhattacharya S, Bonsignore MR, Dewachter L, Dinh-Xuan AT, Dorfmüller P et al. Pulmonary vascular endothelium: the orchestra conductor in respiratory diseases: highlights from basic research to therapy. Eur Respir J 2018, 51.
54. Seimetz M, Parajuli N, Pichl A, Veit F, Kwapiszewska G, Weisel FC, Milger K, Egemnazarov B, Turowska A, Fuchs B, et al. Inducible NOS inhibition reverses tobacco-smoke-induced emphysema and pulmonary hypertension in mice. Cell. 2011;147:293–305.
55. Davel AP, Lemos M, Pastro LM, Pedro SC, de André PA, Hebeda C, Farsky SH, Saldiva PH, Rossoni LV. Endothelial dysfunction in the pulmonary artery induced by concentrated fine particulate matter exposure is associated with local but not systemic inflammation. Toxicology. 2012;295:39–46.
56. Thiele M, Donnelly SC, Mitchell RA. OxMIF: a druggable isoform of macrophage migration inhibitory factor in cancer and inflammatory diseases. J Immunother Cancer 2022, 10.

57. Chen S, Yan D, Qiu A. The role of macrophages in pulmonary hypertension: Pathogenesis and targeting. Int Immunopharmacol. 2020;88:106934.
58. Alkhanfar D, Shahin Y, Alandejani F, Dwivedi K, Alabed S, Johns C, Lawrie A, Thompson AAR, Rothman AMK, Tschirren J et al. Severe pulmonary hypertension associated with lung disease is characterised by a loss of small pulmonary vessels on quantitative computed tomography. ERJ Open Res 2022, 8.
59. Shahin Y, Alabed S, Alkhanfar D, Tschirren J, Rothman AMK, Condliffe R, Wild JM, Kiely DG, Swift AJ. Quantitative CT evaluation of small pulmonary vessels has functional and prognostic value in Pulmonary Hypertension. Radiology. 2022;305:431–40.
60. Koutros S, Graubard B, Bassig BA, Vermeulen R, Appel N, Hyer M, Stewart PA, Silverman DT. Diesel Exhaust exposure and cause-specific mortality in the Diesel Exhaust in Miners Study II (DEMS II) cohort. Environ Health Perspect. 2023;131:87003.
61. Ferguson JM, Costello S, Elser H, Neophytou AM, Picciotto S, Silverman DT, Eisen EA. Chronic obstructive pulmonary disease mortality: the Diesel Exhaust in Miners Study (DEMS). Environ Res. 2020;180:108876.
62. Armah EK, Adedeji JA, Boafo BB, Opoku AA. Underground Gold Miner exposure to noise, Diesel Particulate matter and crystalline silica dust. J Health Pollut. 2021;11:210301.

Publisher's note